

Experimental demonstration of one-dimensional active plate-type acoustic metamaterial with adaptive programmable density

Ahmed Allam,^{1, 2, a)} Adel Elsabbagh,^{1, 3} and Wael Akl^{1, 3}

¹⁾ Group for Advanced Research in Dynamic Systems, Ain Shams University, Cairo 11517, Egypt

²⁾ Mechatronics Department, Ain Shams University, Cairo 11517, Egypt

³⁾ Design and Production Engineering Department, Ain Shams University, Cairo 11517, Egypt.

(Dated: February 26, 2017)

A class of active acoustic metamaterials (AMMs) with a fully controllable effective density in real-time is introduced, modeled and experimentally verified. The density of the developed AMM can be programmed to any value ranging from -100 kg/m³ to 100 kg/m³ passing by near zero density conditions. This is achievable for any frequency between 500 and 1500 Hz. The material consists of clamped piezoelectric diaphragms with air as the background fluid. The dynamics of the diaphragms are controlled by connecting a closed feedback control loop between the piezoelectric layers of the diaphragm. The density of the material is adjustable through an outer adaptive feedback loop that is implemented by the real-time evaluation of the density using the 4-microphone technique. Applications for the new material include programmable active acoustic filters, non symmetric acoustic transmission and programmable acoustic superlens.

Keywords: Acoustics; metamaterials; piezoelectric materials

ACCEPTED

^{a)} Author to whom correspondence should be addressed. Electronic mail: a.allam@eng.asu.edu.eg

INTRODUCTION

Acoustic metamaterials (AMMs) have been the focus of a lot of theoretical and experimental work in the past few years. The ability to construct materials with properties that are not available in nature has opened the way to the fabrication of acoustic devices that were once thought impossible to achieve. Acoustic superlens^{1–3}, acoustic cloacks^{4–7}, non reciprocal transmission^{8,9}, extraordinary sound absorption^{10–12} and transmission¹³ are all examples of once thought impossible devices. Ever since Liu et al.¹⁴ have realised the first AMM in the form of rubber coated lead balls, a lot of different classes of AMMs have been proposed and analyzed. This includes space coiling AMMs^{15–17}, AMMs based on phononic crystals^{18–20} and resonant AMMs^{21–23}.

Elastic membranes and plates have been widely used to design resonant AMMs²⁴. Membrane- and plate-type AMMs are known for having a simple structure and for being lightweight. They can normally obtain negative effective mass density at low frequencies²¹ enabling them to achieve extraordinary sound absorption^{10,11} and insulation^{25,26}, especially at low frequencies^{27,28}. They can also achieve near zero effective density, a phenomenon with many interesting applications regarding the control of sound propagation^{7,13,29}. The resonant nature of membrane-type AMMs, however, limits their extraordinary properties to narrow frequency bands. The material has to be carefully manufactured and tuned to target a particular band.

The material properties of AMMs can be manipulated by embedding active elements inside their structure (active AMMs). This manipulation of properties is done by an external voltage signal and is hardly available in any natural material. This enables the construction of interesting acoustic reconfigurable and programmable devices^{9,30}. Different types of active AMMs have been proposed. This includes using Helmholtz resonators with piezoelectric diaphragms³¹, acoustic cavities with piezoelectric diaphragm at both ends^{32–34}, magnetorheological elastomer membrane³⁵, layered piezoelectric material^{36–38}, decorated membrane controlled by an electric field³⁹, elastic membranes tensioned by direct current electromagnets⁴⁰ and composite piezoelectric-lead plates⁴¹. All these approaches however are limited to tuning the original properties of the material by shifting the dispersion plots. Popa et al.⁴² suggested a design for a tunable active AMM consisting of a piezoelectric diaphragm and a unidirectional electret transducer. The signal measured from the transducer is used to drive

piezoelectric diaphragm after passing by a reconfigurable electronic circuit, they later modified this design to include sensing element in the piezoelectric diaphragm^{9,43}. Through manipulating the electronic circuit, they were able to control the frequency dependent properties of the cell and use it in the design of a reconfigurable beam steering device and acoustic lens⁴³. As with the previous designs, although Popa et al. used a feedback circuit to manipulate the properties of the device, they didn't show a way to directly set the properties of their cell to a particular value; moreover, their design is of open loop nature in the sense that their effective properties can be changed, but they cannot be directly guaranteed in a closed loop sense.

In the current work, an active one-dimensional (1D) AMM is proposed. Its effective density can be controlled and programmed to a desired set value. The material unit cell consists of a circular composite piezoelectric plate clamped in air. The diaphragm consists of two piezoelectric layers with a brass layer in the middle. The dynamic properties of the material are manipulated by constructing a feedback loop by measuring the voltage generated by one of the layers and applying a control signal to the other layer. A vibro-acoustic analytic model is developed to analyze the behavior of the proposed AMM. A single cell of the proposed AMM is fabricated and an experimental setup is constructed to verify the material properties of the AMM. Several designs for the control system of the cell are proposed and their performance is evaluated. The effective density of the cell is then controlled using an outer control loop with an adaptive control algorithm that estimates the density of the material and applies a control voltage to the cell to achieve the desired density value.

This work is divided into eight sections. In Section II, the structure of the unit cell of the AMM is introduced. In Section III, an analytic model for the prediction of the material properties of the introduced AMM is discussed. In Section IV, the stability of the AMM cell under closed loop operation is discussed. In Section V, a test setup for the experimental evaluation of the material properties of the suggested AMM is introduced and the experimental and analytic results are compared. In Section VI, several types of controllers for the AMM cell are discussed and their performance is evaluated. In Section VII a closed feedback loop for controlling the density of the AMM cell through an adaptive control algorithm is introduced.

Table I. Properties of the materials used in the construction of the AMM cell.

Property	Unit	PZT-4	Brass	Silver
ρ	kg/m ³	7500	8750	10490
C_{11}	GPa	139	169	125
C_{12}, C_{23}	GPa	78	87	74
C_{33}	GPa	115	169	125
e_{31}	C/m ²	-5.2	-	-
e_{33}	C/m ²	15	-	-
ϵ_{11}		1475	-	-
ϵ_{33}		1300	-	-

II. MATERIAL CONSTRUCTION

The suggested one-dimensional active metamaterial consists of an array of clamped piezoelectric diaphragms (piezoelectric buzzers) with air as the background material. The material is formed by repeating the unit cell shown in Figure 1 along the shown propagation (x) direction. The unit cell consists of circular piezoelectric diaphragm clamped along the circumference at a diameter of 38 mm and the unit cell has a total length of 10 mm along the propagation direction. This corresponds to a homogenization limit around 3400 Hz, assuming the length of the unit cell (a) is, at least, an order of magnitude less than the wavelength of incident waves in air. The diaphragm consists of three layers; a brass disk of thickness 140 μm in the middle with two piezoelectric layers, each of thickness 140 μm , deposited on each side. The piezoelectric layers are made from PZT-4 material and they have a diameter of 30 mm. They are covered with silver electrodes of thickness 10 μm from the external sides. The electrodes cover a circle of diameter 28 mm. The material properties of the different components of the cell are summarized in Table I, where the subscript 3 denotes to the polarization direction of the piezoelectric layers which is normal to the plane of the diaphragm and the subscripts 1 and 2 denote to the properties in the plane of the diaphragm.

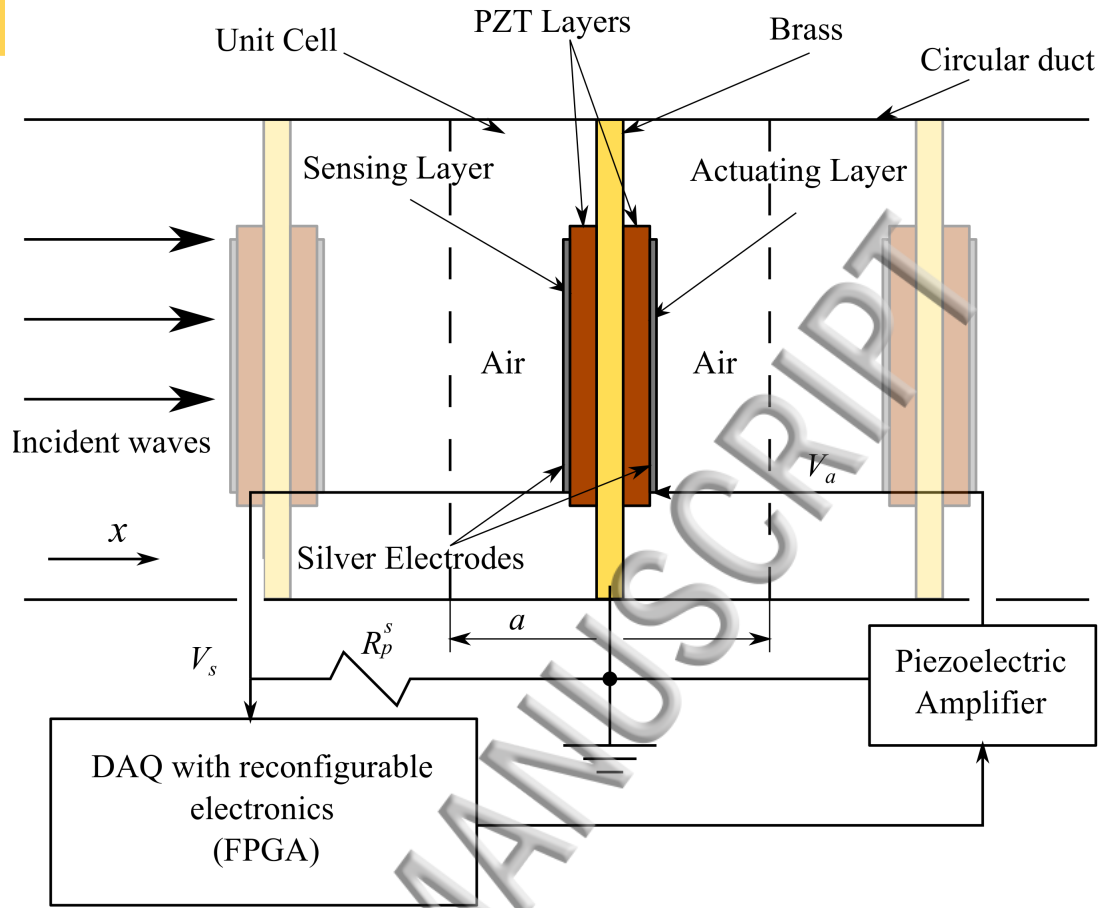


Figure 1. Schematic for the construction of the suggested 1D AMM with one unit cell of the material highlighted.

III. THEORETICAL FORMULATION

A. Two-port Model

The unit cell is modeled and homogenized using the acoustic two-port theory commonly used to analyze the propagation of plane sound waves in ducts. The propagation of the acoustic waves in an acoustic element with two ports a and b can be described by the transfer matrix \mathbf{T} :

$$\begin{bmatrix} p_a \\ v_a \end{bmatrix} = \mathbf{T} \begin{bmatrix} p_b \\ v_b \end{bmatrix} \quad (1)$$

where p_a, v_a, p_b, v_b are the acoustic pressure and particle velocity at ports a and b . The AMM unit cell will be considered as a network of acoustic elements consisting of two homogeneous air layers, with the piezoelectric diaphragm as a third layer in the middle. The transfer

matrix of the cell \mathbf{T}_{cell} is calculated by multiplying the transfer matrix of each of its layers.

$$\mathbf{T}_{cell} = \mathbf{T}_{air}\mathbf{T}_{dia}\mathbf{T}_{air} \quad (2)$$

where \mathbf{T}_{air} is the transfer matrix of each air layer and \mathbf{T}_{dia} is the transfer matrix of the diaphragm. \mathbf{T}_{cell} can be used to calculate the scattering matrix of the cell \mathbf{S}_{cell} ⁴¹. The scattering matrix has the form:

$$\mathbf{S} = \begin{bmatrix} S_{11} & S_{12} \\ S_{21} & S_{22} \end{bmatrix} \quad (3)$$

where the elements of the scattering matrix S_{11} and S_{22} represent the complex pressure reflection coefficients for waves incident from both sides. Similarly S_{12} and S_{21} represent the complex pressure transmission coefficients. The S_{11} and S_{12} of the cell can be used to evaluate the effective material properties of the developed AMM. This is done using an inverse program based on the retrieval method introduced by Fokin et al.⁴⁴. The results of this method could be misinterpreted if not examined carefully^{45–47} and other retrieval methods exist^{48,49}. While they can produce results which are less prone to misinterpretations, they are usually limited to analytic formulas and are difficult to be used in practice. Using Fokin's retrieval method, the effective impedance Z_{eff} and refractive index n_{eff} of the material can be calculated from⁴⁴:

$$n_{eff} = \frac{-j \ln(\phi) + 2\pi m}{k_o a}, \quad Z_{eff} = \frac{\rho_o c_o q}{1 - 2S_{11} + S_{11}^2 - S_{12}^2} \quad (4)$$

where k_o , ρ_o , c_o are respectively the wavenumber, density and speed of sound in air, m is the branch number, j is the engineering complex number assuming the fields has a time dependence of $e^{j\omega t}$, and:

$$q = \pm \sqrt{(S_{11}^2 - S_{12}^2 - 1)^2 - 4S_{12}^2}, \quad \phi = \frac{1 - S_{11}^2 + S_{12}^2 + q}{2S_{12}} \quad (5)$$

The effective density and the effective bulk modulus of the AMM (ρ_{eff} , B_{eff}) can be calculated from Z_{eff} , n_{eff} from:

$$\rho_{eff} = \frac{n_{eff} Z_{eff}}{c_o}, \quad B_{eff} = \frac{Z_{eff} c_o}{n_{eff}} \quad (6)$$

The effective material properties of the cell are controlled by manipulating the dynamics of the diaphragm through the voltage signals applied to the piezoelectric layers. Since the

thickness of the diaphragm is very thin compared to the total thickness of the cell, it will be considered as a lumped acoustic impedance (Z_{dia}) and \mathbf{T}_{dia} is then given by:

$$\mathbf{T}_{dia} = \begin{bmatrix} 1 & Z_{dia} \\ 0 & 1 \end{bmatrix} \quad (7)$$

In the following section the active acoustic impedance of the diaphragm is estimated from the deflection of the diaphragm.

B. Acoustic impedance of the piezoelectric diaphragm

The piezoelectric diaphragm is considered as a laminated plate. The laminae of the investigated diaphragm are transversely isotropic, have the same orientation, and their distribution about the mid-plane is symmetric. Also, it is only subjected to axisymmetric loads. The equations of motion of the diaphragm in the transverse and the in-plane directions are hence given in polar coordinates by⁵⁰

$$(D_{11}\nabla^4 - N^P\nabla^2 + m_o\frac{\partial^2}{\partial t^2})w(r, t) = p_i(t) + f_3^P(t) \quad (8)$$

$$(A_{11}\nabla^2 - \frac{1}{r^2} - m_o\frac{\partial^2}{\partial t^2})u(r, t) = f_1^P(t) \quad (9)$$

where ∇^4 is the bi-harmonic operator, ∇^2 is the Laplacian operator, w is the transverse deflection of the plate, u is the in-plane deflection in the radial direction, r is the radial position measured from the center of the plate, N^P are the in-plane forces, $p_i(t)$ is the acoustic pressure incident on the diaphragm, A_{ij} are the extensional stiffnesses and D_{ij} are the bending stiffnesses, m_o is the mass per unit area of the plate. The terms f_i^P are determined from the resultant forces N^P and moments M^P induced by the piezoelectric effect:

$$f_1^P = \nabla^2 N^P, \quad f_3^P = -\nabla^2 M^P \quad (10)$$

where N^P, M^P are the resultant forces and moments due to the piezoelectric effect:

$$N^P = \sum_{k=1}^N \int_{z_k}^{z_{k+1}} \bar{e}_{31}^{(k)} \mathcal{E}_3^{(k)} dz \quad (11)$$

$$M^P = \sum_{k=1}^N \int_{z_k}^{z_{k+1}} \bar{e}_{31}^{(k)} \mathcal{E}_3^{(k)} z dz \quad (12)$$

where $\mathcal{E}_3^{(k)}$ is the traverse electric filed applied to layer k . When the electric potential applied to the piezoelectric layers is uniform across the area, the terms f_1^P and f_3^P are reduced to zero except at the lateral boundaries of the electrode. Assuming rest initial conditions, Equations (8) and (9) can be converted to the frequency domain by the aid of Laplace transform. The transformed equation is given by:

$$\begin{aligned} (D_{11}\nabla^4 - N^P\nabla^2 + I_0S^2)W(S) &= P_i(S) \\ (A_{11}\nabla^2 - \frac{1}{r^2} - I_0S^2)U(S) &= 0 \end{aligned} \quad (13)$$

The solutions of Equation (13) have the form:

$$\begin{aligned} W(r, S) &= E_1(S)J_0(g_1(S)r) + E_2(S)Y_0(g_1(S)r) \\ &\quad + E_3(S)I_0(g_2(S)r) + E_4(S)K_0(g_2(S)r) \\ &\quad - \frac{P_i(S)}{D_{11}g^4(S)} \\ U(r, S) &= E_5(S)J_1(g_p(S)r) + E_6(S)Y_1(g_p(S)r) \end{aligned} \quad (14)$$

where $J_0()$, $I_0()$, $Y_0()$, $K_0()$ are the zeroth order Bessel and modified Bessel functions of the first and second kind, g is the wave number of the flexural waves traveling through the diaphragm and is given by:

$$g^4 = \frac{-m_oS^2}{D_{11}} \quad (15)$$

g_1, g_2 are given by:

$$g_1^2 = \frac{-N^F + \sqrt{4D_{11}^2g^4 + N^F}}{2D_{11}} \quad (16)$$

$$g_2^2 = \frac{-N^F - \sqrt{4D_{11}^2g^4 + N^F}}{2D_{11}} \quad (17)$$

g_p is defined as:

$$g_p^2 = \frac{-m_oS^2}{A_{11}} \quad (18)$$

$E_1 \dots E_6$ are constants to be determined from the boundary conditions of the plate.

From this point forward, the dependency of the variables on S will be omitted for brevity. Assuming the diaphragm consisting of N_c uniform annular sections. Equation (13) can be solved for each section l and the transverse and in-plane deflections at section l are

given by:

$$W_l(r) = E_{1l}J_0(g_{1l}r) + E_{2l}Y_0(g_{1l}r) + E_{3l}I_0(g_{2l}r) + E_{4l}K_0(g_{2l}r) - \frac{P_i}{D_{11l}g_{kl}^4} \quad (19)$$

$$U_l(r) = E_{5l}J_1(g_{pl}r) + E_{6l}Y_1(g_{pl}r)$$

The constants $E_{1l} \dots E_{6l}$ are determined by the boundary conditions of the diaphragm, in addition to the continuity conditions between each two neighboring sections. The boundary and continuity conditions are hence given by:

$$\begin{aligned} W_1(0) &= \text{finite}, & U_1(0) &= \text{finite} \\ M_l(R_l) &= M_{l+1}(R_l), & Q_l(R_l) &= Q_{l+1}(R_l) \\ W_l(R_l) &= W_{l+1}(R_l), & \left. \frac{\partial W_l}{\partial r} \right|_{R_l} &= \left. \frac{\partial W_{l+1}}{\partial r} \right|_{R_l} \\ U_l(R_l) &= U_{l+1}(R_l), & N_l(R_l) &= N_{l+1}(R_l) \\ W_{N_c}(R_{N_c}) &= 0, & \left. \frac{\partial W_{N_c}}{\partial r} \right|_{R_{N_c}} &= 0, & U_{N_c}(R_{N_c}) &= 0 \end{aligned} \quad (20)$$

where $M_l(r)$ is the moment at section l , $Q_l(r)$ is the shear force at section l , $N_l(r)$ is the harmonic in-plane force. Equations (20) can be reorganized in matrix form:

$$\boldsymbol{\eta} \bar{\mathbf{E}} = \bar{\mathbf{L}}^{P_i} + \bar{\mathbf{L}}^{P_r} \quad (21)$$

where $\boldsymbol{\eta}$ is a $6N_c \times 6N_c$ matrix which is only dependent on the diaphragm properties regardless of the excitation, $\bar{\mathbf{E}}$ is a $6N_c \times 1$ vector of all the unknown constants, $\bar{\mathbf{L}}^{P_i}$ and $\bar{\mathbf{L}}^{P_r}$ are $6N_c \times 1$ load vectors caused by the piezoelectric and the pressure excitations on the diaphragm. The piezoelectric loads depend on the electric circuits connected to the piezoelectric layers. The electric charge generated on the piezoelectric layer k in section l is given in polar form by⁵¹:

$$\begin{aligned} Q_{e_l}^{(k)} &= 2\pi e_{31}^{(k)} \int_{R_{l-1}}^{R_l} \left[r \frac{\partial U_l}{\partial r} + U_l(r) \right] dr \\ &\quad + 2\pi \epsilon_{33}^{(k)} \int_{R_{l-1}}^{R_l} \mathcal{E}_3^{(k)} r dr \\ &\quad - 2\pi e_{31}^{(k)} z^{0(k)} \int_{R_{l-1}}^{R_l} \left[r \frac{\partial^2 W_l}{\partial r^2} + \frac{\partial W_l}{\partial r} \right] dr \end{aligned} \quad (22)$$

where $\epsilon_{33}^{(k)}$ is the electric permittivity under constant stress of piezoelectric layer k and $z^{0(k)}$ is defined by:

$$z^{0(k)} = \frac{z_{k+1} + z_k}{2} \quad (23)$$

For the part of the piezoelectric layers that is fully covered with electrodes, $\mathcal{E}_3^{(k)}$ could be written in terms of the potential difference applied to the layer $V_p^{(k)}$:

$$\mathcal{E}_3^{(k)} = \frac{-V_p^{(k)}}{h^{(k)}} \quad (24)$$

where $h^{(k)}$ is the thickness of layer k . Rewriting Equation (22) in terms of $V_p^{(k)}$ and generated electric current $I_e^{(k)}(S)$:

$$\begin{aligned} I_e^{(k)}(S) &= S Q_e^{(k)}(S) \\ &= 2\pi e_{31} S \int_{R_{l-1}}^{R_l} \left[r \frac{\partial U_l}{\partial r} + U_l(r) \right] dr - C_p^{(k)} S V_p^{(k)} - 2\pi e_{31} z_k^0 S \int_{R_{l-1}}^{R_l} \left[r \frac{\partial^2 W_l}{\partial r^2} + \frac{\partial W_l}{\partial r} \right] dr \end{aligned} \quad (25)$$

where $C_p^{(k)}$ is the electric capacitance of layer k .

Equation (25) can be used to construct the equivalent electric circuit model for piezoelectric layer k , which is shown in Figure 2 where:

$$I_g^{(k)}(S) = 2\pi e_{31} S \int_{R_{l-1}}^{R_l} \left[r \frac{\partial U_l}{\partial r} + U_l(r, S) \right] dr - 2\pi e_{31} z_k^0 S \int_{R_{l-1}}^{R_l} \left[r \frac{\partial^2 W_l}{\partial r^2} + \frac{\partial W_l}{\partial r} \right] dr \quad (26)$$

$I_g^{(k)}$ only depends on the deflections of the diaphragm and not the external circuit, it can be written in matrix form as:

$$I_g^{(k)} = \bar{\alpha}^{(k)} \bar{E} \quad (27)$$

where $\bar{\alpha}$ is a $1 \times N_c$ vector whose elements are evaluated from Equation (26). The value of $V_p^{(k)}$ is determined by the nature of the circuit connect to each layer. Considering Thevenin's equivalent circuit shown in Figure 2 the value of $V_p^{(k)}$ could be determined from:

$$V_p^{(k)} = G_e^{(k)} Z_p^{(k)} I_g^{(k)} + G_e^{(k)} V_s^{(k)} \quad (28)$$

where:

$$G_e^{(k)} = \frac{1}{1 + Z_p^{(k)} C_p^{(k)} S} \quad (29)$$

For the diaphragm shown in Figure 1. The voltage generated by one of the piezoelectric layers (sensing layer) is measured and fed to a network of reconfigurable electronics (G_c) which is connected to a voltage amplifier (G_a). The amplifier applies excitation voltage on the other layer (actuating layer). The presence of the reconfigurable electronics (reconfigurable

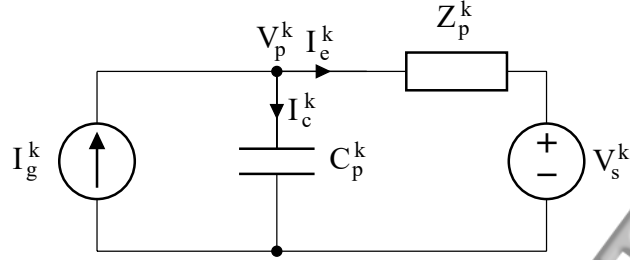


Figure 2. An electrical circuit model for piezoelectric layer k connected to an arbitrary circuit represented by its Thevenin's equivalent

controller) in the loop allows for programming the dynamics of the cell in an arbitrary manner, as long as the stability of the loop is maintained and the maximum allowable excitation voltage is not reached. Applying Equation (28) on the sensing layer results in:

$$V_p^s = G_e^s R_p^s I_g^s \quad (30)$$

Where the superscript (s) indicates the sensing piezoelectric layer. Similarly, for the actuating layer:

$$V_p^a = G_e^a R_p^a I_g^a + G_e^a V_s^a \quad (31)$$

where R_p^a is the output impedance of the piezoelectric amplifier. The applied voltage on the actuating layer V_s^a can be calculated from:

$$V_s^a = G_c G_a V_p^s = G_a G_c G_e^s R_p^s I_g^s \quad (32)$$

Thus:

$$V_p^a = G_e^a R_p^a I_g^a + G_e^a G_a G_c G_e^s R_p^s I_g^s \quad (33)$$

Substituting for I_g^a and I_g^s using Equation (27) in Equation (33) and combining it with Equations (11,12,24), the piezoelectric load vector is then:

$$\bar{L}^{Pi} = \bar{\phi}^s G_e^s R_p^s \bar{\alpha}^s \bar{E} + \bar{\phi}^a G_e^a R_p^a \bar{\alpha}^a \bar{E} + \bar{\phi}^a G_c G_a G_e^a G_e^s R_p^s \bar{\alpha}^s \bar{E} \quad (34)$$

where $\bar{\phi}^s$ and $\bar{\phi}^a$ are $6N_c \times 1$ vectors constructed by substituting by Equations (11,12,24) into Equations (20). They represent the effect of the applied voltage on the two piezoelectric layers on the boundary conditions of the diaphragm. Substituting by Equation (34) in Equation (21) and reorganizing, gives:

$$\eta_o \bar{E} = \bar{\phi}^a G_e^a G_a G_c G_e^s R_p^s \bar{\alpha}^s \bar{E} + \bar{L}^{Pr} \quad (35)$$

where η_o represents the dynamics of the cell with no control action applied on the actuation layer.

$$\eta_o = \eta - \bar{\phi}^s G_e^s R_p^s \bar{\alpha}^s \bar{E} + G_e^a R_p^a \bar{\alpha}^a \bar{E} \quad (36)$$

The dynamics of the closed loop cell are summarized in the block diagram shown in Figure 3.

The unknown coefficients are then given by:

$$\bar{E} = (\eta_o - \bar{\phi}^a G_e^a G_a G_c G_e^s R_p^s \bar{\alpha}^s)^{-1} \bar{L}^{Pr} \quad (37)$$

Now that the unknown coefficients are determined, the average displacement of the diaphragm \widetilde{W} is given by:

$$\widetilde{W} = \frac{1}{A_t} \int_{A_t} W(r) dA \quad (38)$$

where A_t is the total area of the diaphragm. The previous equation could be rewritten in matrix form

$$\widetilde{W} = \bar{\alpha}_p \bar{E} + \gamma \quad (39)$$

Where $\bar{\alpha}_p$ is a $1 \times 6N_c$ vector of the coefficients resulting from Equation (38) and γ represents the feed through terms that don't depend on the boundary conditions. The impedance of the diaphragm is then given by:

$$Z_{dia} = \frac{\widetilde{W}}{P_i} \quad (40)$$

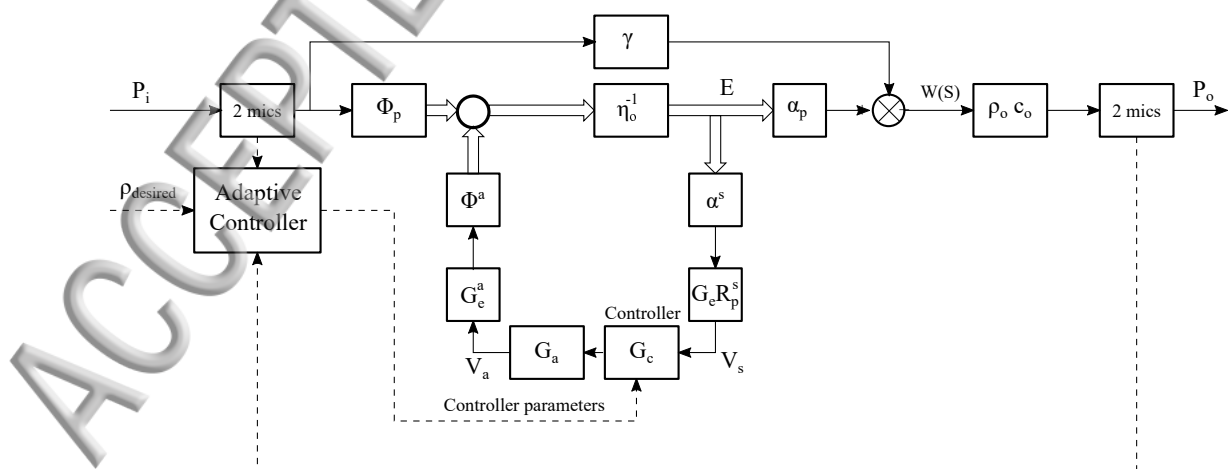


Figure 3. A block diagram representing the dynamics of the closed loop cell with adaptive control

IV. STABILITY OF THE CELL

The controller transfer function G_c can be chosen to set the effective material properties of the AAM to arbitrary values. However, this must be done while keeping the cell stable and avoiding any self-sustained oscillations. This is done by examining the open loop transfer function of the system G_{OL} . From Figure 3, the open loop transfer function of the cell can be calculated from:

$$G_{OL} = G_c G_a G_e^a G_e^s R_p^s \bar{\alpha}^s \eta_o \bar{\phi}^a \quad (41)$$

Since the diaphragm is a continuous structure, the estimation of the stability of the system is not straight forward. The estimated open loop transfer function (G_{OL}) is not rational; hence, it is difficult to estimate the stability of the cell analytically. It is possible however to determine the stability margin of the system graphically by examining the Bode plot of G_{OL} around the frequency region targeted by the controller (G_c). Thus, in order to ensure the stability of the system, G_c should be chosen to have a decaying response outside the targeted frequency region.

V. CHARACTERIZATION OF THE AMM CELL

The test setup shown in Figure 4 is used to characterize the effective material properties of the cell using the two source method⁵². The setup has an inner tube diameter of 25 mm. Three PCB model 378C10 $\frac{1}{4}$ " IEPE microphones are flush mounted to each tube. Two SEAS W18EX001 100W speakers powered by a Yamaha P3500S audio amplifier are used to provide upstream and downstream acoustic excitation. The signals of the microphones are connected to the channels of a NI PXI-4472 eight channel input module mounted on a NI PXI-1042Q data acquisition system. The sensitivity of each microphone is calibrated using a B&K 4231 sound calibrator. The relative phase between them is calibrated using a phase calibrator. The control circuit of the cell is constructed by connecting the signal of the sensing PZT layer to an input channel of an NI PXI-7854R multifunction reconfigurable I/O. The output channel of the NI PXI-7854R is connected to a Piezodrive MX200 200V 1A Piezo Driver, which supplies the voltage signal to the actuating PZT layer.

A single AMM cell is constructed by clamping a AB4113B commercial bender (piezoelectric diaphragm) using the mechanical clamp shown in Figure 4. The diameter of the designed

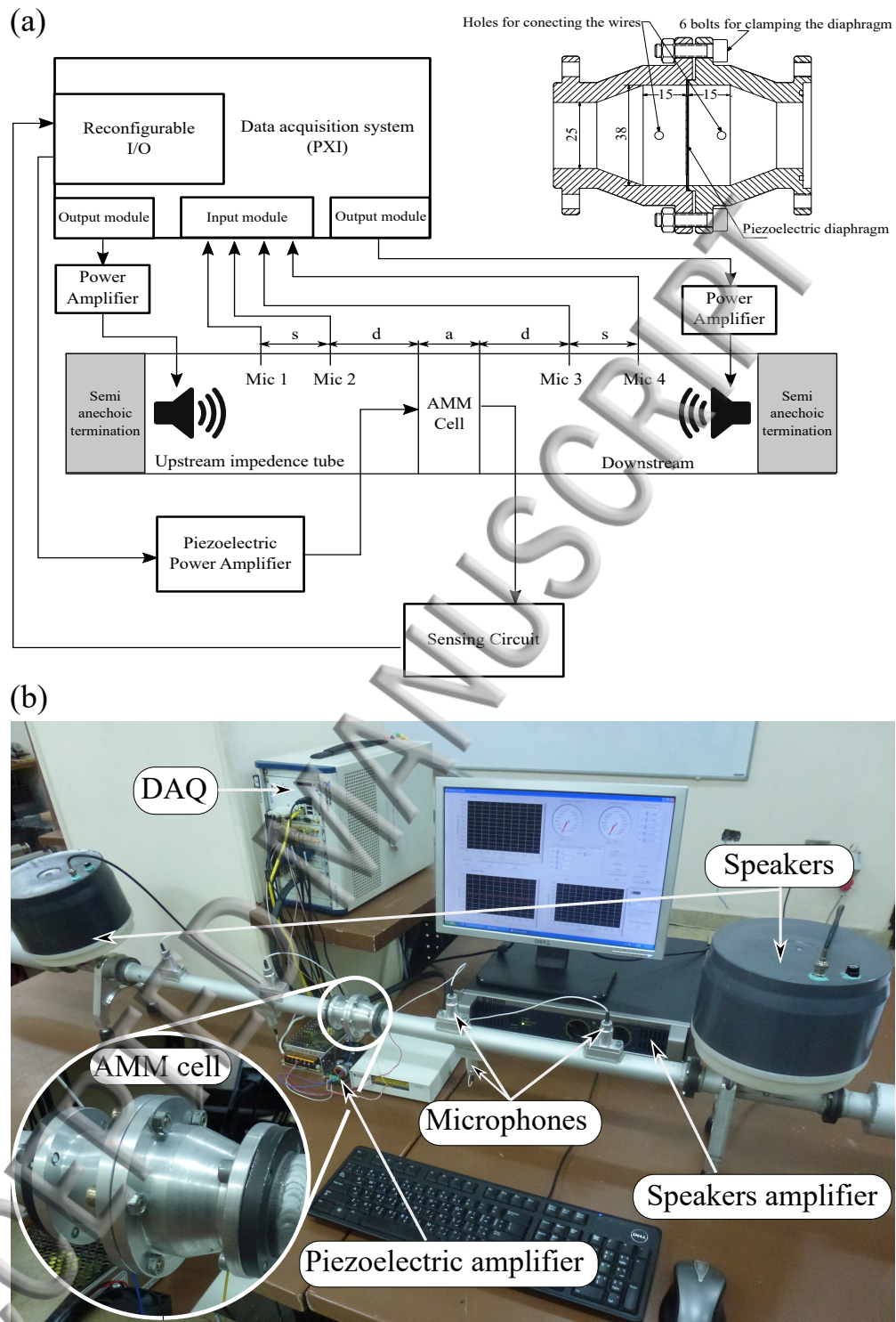


Figure 4. (a) Schematic for the test setup connections and the construction of the AMM cell (b) Photo of the actual test setup.

(38 mm) is different from that of the impedance tubes (25 mm) so the clamp was designed with a cone adaptor to connect the cell to the upstream and downstream impedance tubes. The effective material properties of the cell are determined by exciting the cell with band limited white-noise excitations up to 2000 Hz. For each measurement 100 readings are recorded and averaged to reduce the measurement noise. With the controller gain set to zero, open loop cell, the effective density is estimated experimentally and compared to the analytic results obtained from the developed model (Figure 5). An excellent agreement is observed between the predicted and measured values over the studied frequency range, even though a commercial diaphragm is used and that no special manufacturing techniques were used to ensure its properties. Figure 5 shows that the value of the real component density approaches zero near the first resonance frequency, around 1100 Hz. It changes from large negative values for frequencies below the resonance to large positive values for a certain frequency range above the first resonance. The Transmission Loss (TL) of the cell is shown in Figure 5(c,f). The TL of the cell is defined by:

$$TL = 20 \log_{10} \left(\frac{1}{S_{12}} \right) \quad (42)$$

The TL of the material is minimum near the resonance frequency of the diaphragm, which is expected since the deflection amplitude of the diaphragm should be maximum near its resonance. Similar distributions for the density and TL was repeatedly observed for previous membrane-type AMMs with different configurations^{39,53,54}.

VI. CONTROLLER TRANSFER FUNCTION

The relation between the effective density and the frequency suggests that shifting the first resonance to lower or higher frequencies would allow for controlling the effective density within a limited frequency range near the resonance of the cell. This shift could be done using a lead-lag controller with the following transfer function:

$$G_c = \frac{K_c(S + z_1)}{(S + p_1)(S + p_2)} \quad (43)$$

The value of the gain K_c controls the amount of the shift and its sign controls its direction, where the locations of the poles (p_1, p_2) and the zero (z_1) are chosen to maximize the allowable frequency shift before the system becomes unstable. This controller approach however

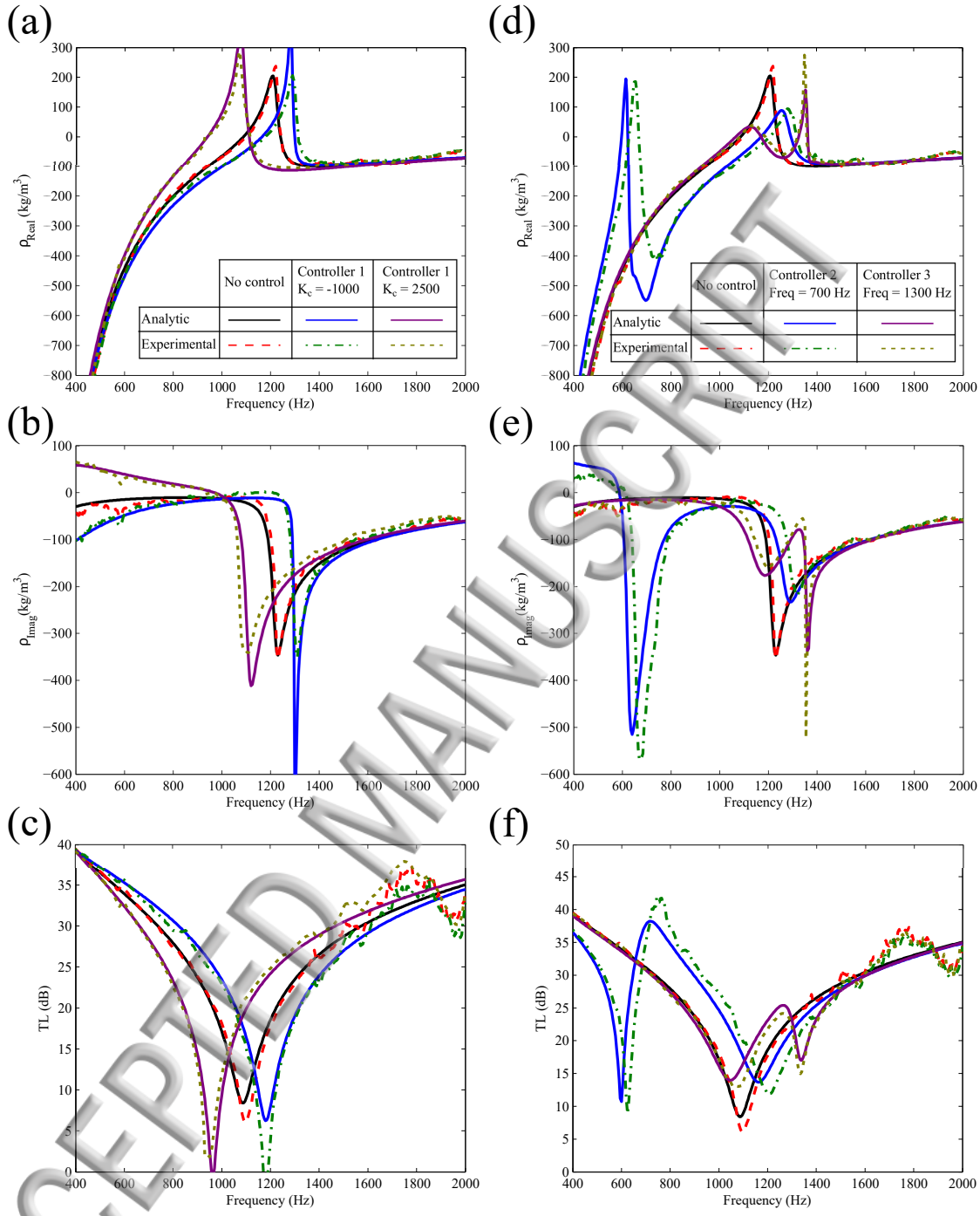


Figure 5. The real and imaginary components of the effective density, as well as, the TL of the developed AMM characterized analytically and experimentally. The results obtained without any control applied to the cell are compared to those obtained (a,b,c) using controller 1 (Equation (43)) with $K_c = -1000$ and $K_c = 2500$ and (d,e,f) using controller 2 (Equation (44)) with $f_c = 700 \text{ Hz}$ and $K_c = 4 \times 10^6$ and controller 3 (Equation (45)) with $f_c = 1300 \text{ Hz}$ and $K_c = -120$.

limits the controllable frequency range to a small region around the open loop resonance of the diaphragm. The effect of applying this controller to the cell is shown in Figure 5(a,b,c). The parameters of the controller were set to $z_1 = 1000$, $p_1 = p_2 = -4500$ and K set to 2500 for negative shift and -1000 for positive shift of the resonance. Good agreement between the predicted and measured effective density was observed for both negative and positive frequency shift controller configurations.

An alternative approach would be to set the transfer function of the controller so that it adds an additional resonance frequency to the closed loop transfer function. This induces a similar behavior to what happens near the open loop resonance at the selected additional frequency. For frequencies below the open loop resonance, this could be done by setting the transfer function of the controller G_c to:

$$G_c = \frac{K_c}{S^2 + 2\zeta_c\omega_c S + \omega_c^2} \quad (44)$$

where $\omega_c = 2\pi f_c$ and f_c is calculated from the target resonant frequency of the controller in Hz, ζ_c is damping ratio of the controller and K_c is the controller gain. In order to control the density of the cell around a certain target frequency, ω_c of the controller could be initially set to match this frequency. By shifting ω_c to higher or lower values, the effective density could be fully controlled within the reachable limits of the controller. These limits are bounded by the values of K_c and ζ_c which maintain the system's stability. If the target frequency is above the open loop resonance, the transfer function could be set to:

$$G_c = \frac{K_c(S - z_1)}{S^2 + 2\zeta_c\omega_c S + \omega_c^2} \quad (45)$$

where (z_1) is an additional zero, used to tune the phase of the open loop transfer function of the system to ensure its stability. Figure 5(d,e,f) shows the effect of setting the controller transfer function to the resonant controllers (Equation (44) with $\zeta_c = 0.04$, $K_c = 4 \times 10^6$ and $f_c = 700$ Hz and Equation (45) $\zeta_c = 0.04$, $K_c = -120$ and $f_c = 1300$ Hz) on the effective density of the cell. The analytic model succeeds in the estimation of the general behavior of the properties cell under the effect of the two controllers. The resonant controllers achieve their target objective by adding an additional zero-crossing frequency (additional resonance) near the frequency which they are targeting. The value of the imaginary component of the density shown in Figure 5(b,d) is negative for the studied frequency range in the uncontrolled case. This condition must be present to ensure that the used homogenization technique did

not violate any passivity conditions found in the material. For the controlled cases the imaginary component of the density is positive at certain frequency ranges, which indicates that the material is no longer passive at these regions (gain medium) and that the energy supplied to the system by the control action is greater than the losses inside the material.

VII. ADAPTIVE CONTROL OF THE CELL DENSITY

The ability to measure the density of the cell in real-time allows for adapting the parameters of the controller transfer function to achieve a desired density at a specific frequency. This first requires the density of the cell to be estimated in real-time. A density estimator is developed based on the same two-source method⁵² used in the measurements. Two microphones at each side of the cell are used to decompose the acoustic waves passing through the cell and estimate its real-time reflection and transmission coefficients. The two source method however requires the cell to be excited at least once from each side to evaluate the 4 elements of the scattering matrix. To overcome this limitation, the fact that the cell is symmetrical in the propagation direction will be used to reduce the number of excitations to one. This means that the elements of the scattering matrix could be evaluated in the presence of incident acoustic waves from any direction. The signals acquired from the microphones are sampled with a constant sampling time (T_s) until a predetermined number of samples, time window (T_w), are acquired. The window is then converted to the frequency domain, and the transfer functions between the microphones are determined and converted to the reflection and transmission coefficients of the cell⁵⁵. These coefficients are then fed to an inverse program which is based on the retrieval method developed by Fokin et al.⁴⁴ to estimate the real-time effective density of the cell. An adaptive control algorithm is designed to use the frequency content of the incident waves to determine the dominant frequency of the acoustic waves passing through the cell. It then uses the density estimator to determine the effective density of the cell. Knowing the error between the desired effective density and the required density, it uses a traditional PID controller to adjust the parameters of the feedback controller (G_c). A discrete PID controller is used to tune the parameters of the feedback controller. The resonant controller frequency ω_c is determined from the following relation:

$$\omega_c = \omega_{co} + \Delta\omega_c \quad (46)$$

Where ω_{c_o} is the detected frequency of the incident excitation and $\Delta\omega_c$ is the output of the PID controller.

$$\Delta\omega_c = K_p + \frac{K_i T_w z}{z - 1} + \frac{K_d N(z - 1)}{(1 + N T_w) z - 1} \quad (47)$$

Where K_p , K_i and K_d are the proportional, integral and differential gains of the controller, z is the z-transform variable and N is the cutoff frequency of the low pass filter of the derivative term. The gains of the PID controller, as well as the gain of the resonant controller (K_c), are determined based on the incident frequency (ω_{c_o}) from a set of tuned values which are determined offline for each frequency range separately. The damping of the controller (ζ_c) is kept constant for all controllers.

In order to realize the adaptive controller, the signals of the microphones used in the measurement process are branched and connected to a second NI PXI-4472 eight channel input module mounted on the data acquisition system. The readings from the first input module are used in the measurement process, while those of the second input module are used in the control process. This was done on the hardware level to ensure the complete separation between the two processes.

The adaptive control algorithm is implemented as a standalone C program using the NI Labwindows/CVI libraries to interface with the microphones' signal from the input module and to set the parameters of the controller. The flow of the adaptive control algorithm is summarized in Figure 6. In order to test the performance of the adaptive controller the cell is excited using upstream and downstream stepped sine excitations between 500 Hz and 1500 Hz. Each single frequency excitation is applied on the cell for 10 seconds, so that the response of the controller completely settles before recording the measurement data. The effect of applying the adaptive control algorithm on the effective density of the AMM cell is shown in Figure 7(a,b). It shows that the controller is able to achieve any desired density value between -100 kg/m^3 and 100 kg/m^3 including near zero density conditions. This is achievable for any single frequency between 500 Hz and 1500 Hz. For most of the studied frequency range, the controller was able to change the dynamics of the AMM cell to a value within 10% of the desired density set-point regardless of the open loop density value at the targeted frequency. An exception to this are frequencies near 1500 Hz, for a set value of 100 kg/m^3 , the error reaches about 30%. This error appeared because the control effort is not able to drive the AMM cell to the desired set point at this frequency. Thus, the frequencies around 1500 Hz represent the boundary of the controllable region of

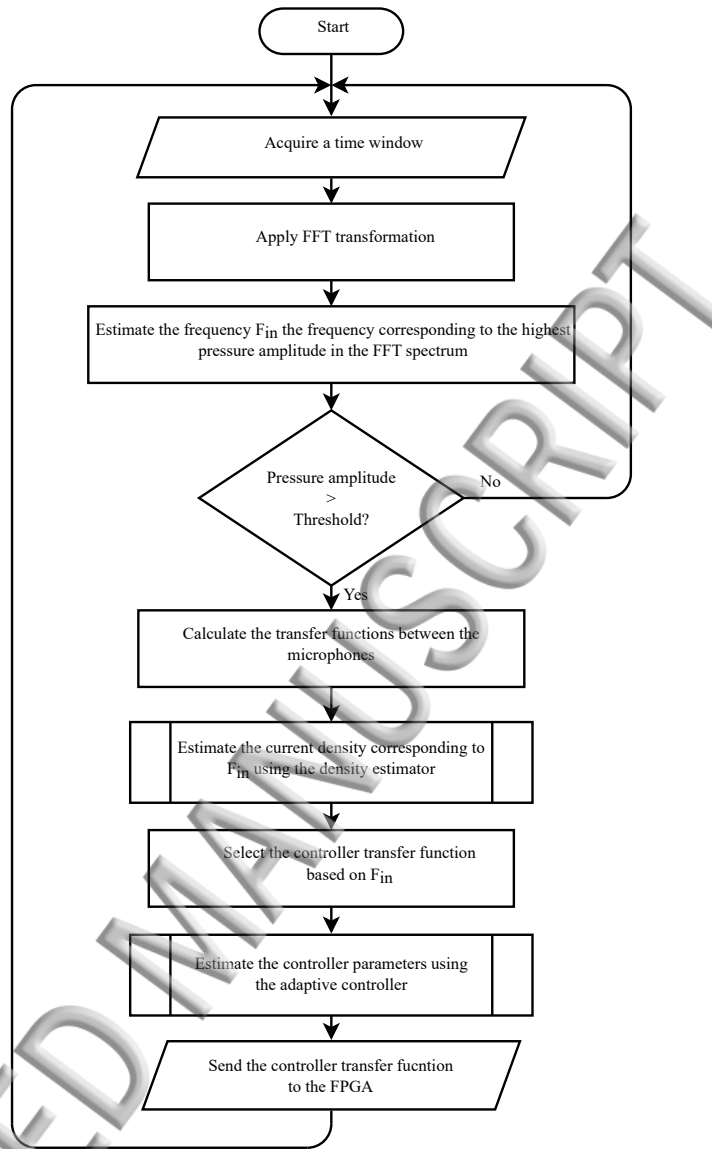


Figure 6. Flowchart for the procedure of the adaption of the cell density based on the incident excitation.

the adaptive controller. The effect of the controller on the bulk modulus of the AMM is shown in Figure 7(c,d). While the controller was able to vary the density between large negative and positive values, the real component of the bulk modulus remained almost constant around that of air $B_o \approx 10^5 \text{ N/m}^2$. This is expected, since membrane-type and plate-type metamaterials are mainly known for unusual effective density²⁴. This is also desirable. The control effort only affects the effective density of the AMM and has minimal side effects on the real component of the effective bulk modulus. An AMM material with fully controllable material properties could be constructed by implementing a hybrid design,

which incorporates another active element to control the bulk modulus. The TL of the closed loop cell under the effect of the controller is shown in Figure 7(e). The TL of the cell was minimal when setting $\rho = 0 \text{ kg/m}^3$, while it was generally higher when setting $\rho = -100 \text{ kg/m}^3$. This further verifies the validity of the homogenization technique used, since $\rho = -100 \text{ kg/m}^3$ should correspond to a stop band in the material while $\rho = 0 \text{ kg/m}^3$ indicates a transmission with zero phase and minimal impedance mismatch with the air. The achieved performance of the AMM cell opens the door to a set of possible applications for the developed material. Asymmetric transmission of acoustic waves could be easily achieved for single tone excitations. Given that the excitation is of a single sided nature, the material could be programmed to detect the propagation direction of the incident waves and adjust its density accordingly. The material could be programmed to work as an active acoustic filter with arbitrary stop (negative density) and pass (near zero density) bands within the material's controllable frequency range. The material could be also programmed to achieve any desired density gradient, given that a sufficient number of cells is used.

VIII. CONCLUSION

A design for a one-dimensional active acoustic plate-type metamaterial is introduced. The material consists of clamped composite piezoelectric diaphragms suspended in air. The effective density of the material is manipulated by adjusting the dynamic properties of the diaphragms through a closed loop feedback controller. An analytic model based on the acoustic two-port theory and the composite laminated plate theory is developed to predict the behavior of the AMM. Three different types of controllers for manipulating the material properties of the cell are introduced. An experimental test setup for the evaluation of the material properties of the AMM is constructed to verify the analytic results. Good agreement is observed between the measured and predicted values for the open loop cell. The proposed resonant feedback controllers are verified to add an additional predetermined resonance frequency to the cell and thus add a new zero-crossing point for the effective density of the material. An adaptive control algorithm is developed to achieve a closed loop control over the density of the AMM. The algorithm estimates the density of the AMM in real-time and adjusts the feedback control transfer function to reach a predetermined value for density of the material at the frequency corresponding to maximum incident acoustic

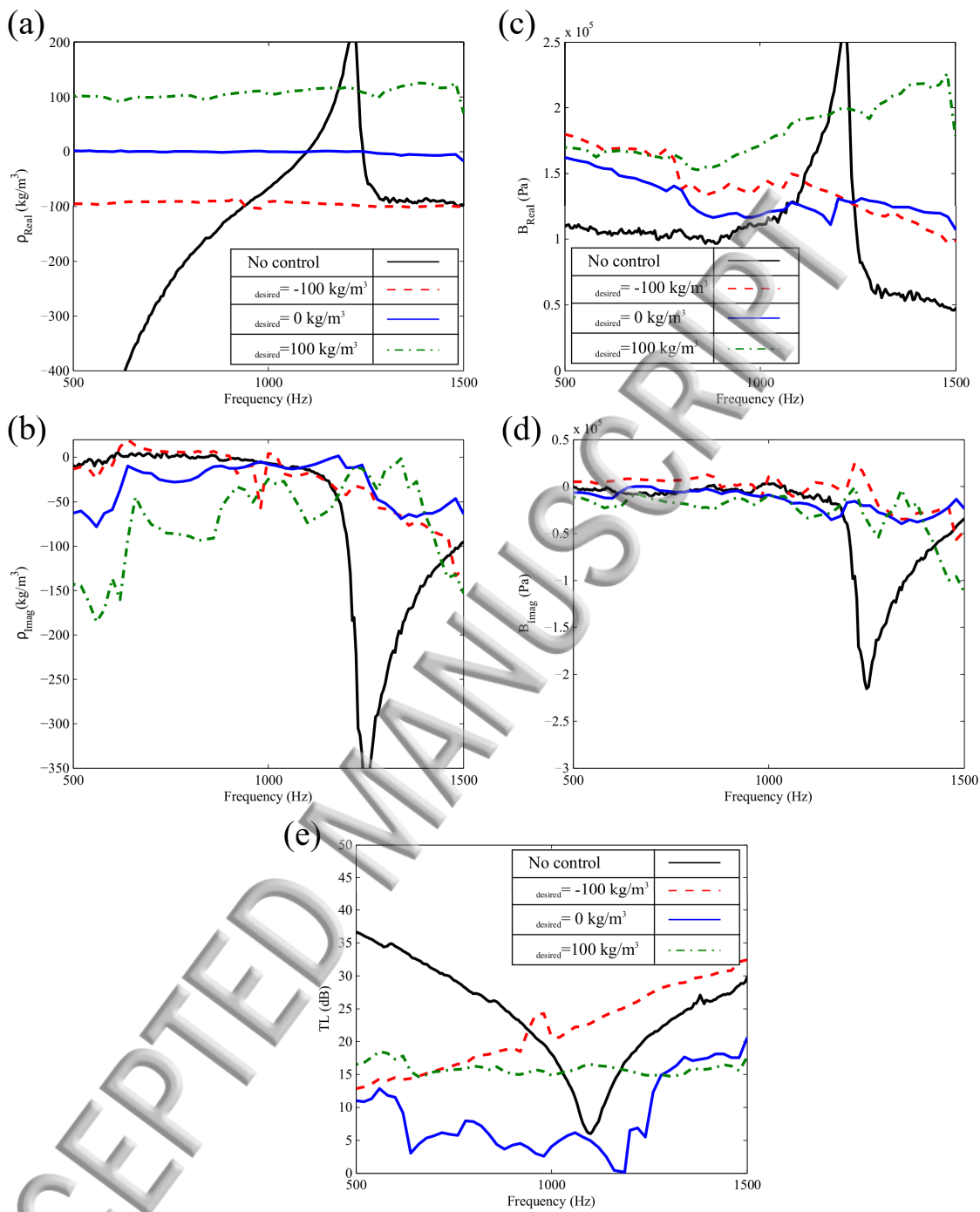


Figure 7. The adaptive controller is tested under three different set points for the density which are $\rho_{\text{desired}} = -100 \frac{\text{kg}}{\text{m}^3}$, $\rho_{\text{desired}} = 0 \frac{\text{kg}}{\text{m}^3}$ and $\rho_{\text{desired}} = 100 \frac{\text{kg}}{\text{m}^3}$. The effect of the controller on the (a) real and (b) imaginary components of the effective density, the (c) real and (d) imaginary components of the bulk modulus and (e) the TL of the closed loop AMM cell are demonstrated. The measured open loop parameters are also plotted as a reference.

sure amplitude. The adaptive controller was proven experimentally to set the density of the cell to values ranging from -100 kg/m^3 up to 100 kg/m^3 for acoustic waves with frequency between 500 and 1500 Hz. Potential applications for the developed material include controllable asymmetric sound transmission, programmable active filters and in the manufacturing of a programmable acoustic superlens.

REFERENCES

- ¹J. Li, L. Fok, X. Yin, G. Bartal, and X. Zhang, *Nat Mater* **8**, 931 (2009).
- ²J. J. Park, C. M. Park, K. J. B. Lee, and S. H. Lee, *Appl. Phys. Lett.* **106**, 051901 (2015).
- ³N. Kaina, F. Lemoult, M. Fink, and G. Lerosey, *Nature* **525**, 77 (2015).
- ⁴S. A. Cummer and D. Schurig, *New J. Phys.* **9**, 45 (2007).
- ⁵S. Cummer, B.-I. Popa, D. Schurig, D. Smith, J. Pendry, M. Rahm, and A. Starr, *Phys. Rev. Lett.* **100**, 024301 (2008).
- ⁶D. Torrent and J. Sánchez-Dehesa, *New J. Phys.* **10**, 063015 (2008).
- ⁷J. Zhao, Z. N. Chen, B. Li, and C.-W. Qiu, *J. Appl. Phys.* **117**, 214507 (2015).
- ⁸B. Liang, B. Yuan, and J.-c. Cheng, *Phys. Rev. Lett.* **103**, 104301 (2009).
- ⁹B.-I. Popa and S. A. Cummer, *Nat. Commun.* **5**, 3398 (2014).
- ¹⁰J. Ma, M. B. Steer, and X. Jiang, *Appl. Phys. Lett.* **106**, 111903 (2015).
- ¹¹M. Fink, *Nat Mater* **13**, 848 (2014).
- ¹²J.-P. Groby, W. Huang, A. Lardeau, and Y. Aurégan, *J. Appl. Phys.* **117**, 124903 (2015).
- ¹³R. Fleury and A. Alù, *Phys. Rev. Lett.* **111**, 055501 (2013).
- ¹⁴Z. Liu, X. Zhang, Y. Mao, Y. Y. Zhu, Z. Yang, C. T. Chan, and P. Sheng, *Science* **289**, 1734 (2000).
- ¹⁵Y. Li, B. Liang, X. Tao, X.-f. Zhu, X.-y. Zou, and J.-c. Cheng, *Appl. Phys. Lett.* **101**, 233508 (2012).
- ¹⁶Z. Liang and J. Li, *Phys. Rev. Lett.* **108**, 114301 (2012).
- ¹⁷S. K. Maurya, A. Pandey, S. Shukla, and S. Saxena, *Sci. Rep.* **6**, 33683 (2016).
- ¹⁸D. Torrent and J. Sánchez-Dehesa, *Phys. Rev. B* **74** (2006), 10.1103/PhysRevB.74.224305.
- ¹⁹D. Torrent and J. Sánchez-Dehesa, *New J. Phys.* **10**, 023004 (2008).
- ²⁰D. Torrent and J. Sánchez-Dehesa, *Phys. Rev. Lett.* **105**, 174301 (2010).

- ²¹G. H. Lee, C. M. Park, Y. M. Seo, Z. G. Wang, and C. K. Kim, *Phys. Lett. A* **373**, 4464 (2009).
- ²²F. Bongard, H. Lissek, and J. Mosig, *Phys. Rev. B* **82**, 094306 (2010).
- ²³L. Fok and X. Zhang, *Phys. Rev. B* **83**, 214304 (2011).
- ²⁴T.-Y. Huang, C. Shen, and Y. Jing, *J. Acoust. Soc. Am.* **139**, 3240 (2016).
- ²⁵C. J. Naify, C.-M. Chang, G. McKnight, and S. Nutt, *J. Appl. Phys.* **108**, 114905 (2010).
- ²⁶C. J. Naify, C.-M. Chang, G. McKnight, F. Scheulen, and S. Nutt, *J. Appl. Phys.* **109**, 104902 (2011).
- ²⁷N. Sui, X. Yan, T.-Y. Huang, J. Xu, F.-G. Yuan, and Y. Jing, *Applied Physics Letters* **106**, 171905 (2015).
- ²⁸L. Fan, Z. Chen, S.-y. Zhang, J. Ding, X.-j. Li, and H. Zhang, *Applied Physics Letters* **106**, 151908 (2015).
- ²⁹Y. Gu, Y. Cheng, J. Wang, and X. Liu, *J. Appl. Phys.* **118**, 024505 (2015).
- ³⁰F. Casadei, T. Delpero, A. Bergamini, P. Ermanni, and M. Ruzzene, *J. Appl. Phys.* **112**, 064902 (2012).
- ³¹W. Akl and A. Baz, *J. Intel. Mat. Sys. Str.* **21**, 541 (2010).
- ³²A. Baz, *New J. Phys.* **11**, 123010 (2009).
- ³³W. Akl and A. Baz, *J. Dyn. Sys., Meas., Control* **134**, 061001 (2012).
- ³⁴W. Akl and A. Baz, *J. Appl. Phys.* **112**, 084912 (2012).
- ³⁵X. Chen, X. Xu, S. Ai, H. Chen, Y. Pei, and X. Zhou, *Appl. Phys. Lett.* **105**, 071913 (2014).
- ³⁶Y. Jin, B. Bonello, and Y. Pan, *J. Phys. D: Appl. Phys.* **47**, 245301 (2014).
- ³⁷A. A. Kutsenko, A. L. Shuvalov, O. Poncelet, and A. N. Darinskii, *J. Acoust. Soc. Am.* **137**, 606 (2015).
- ³⁸Z. Hou and B. M. Assouar, *Appl. Phys. Lett.* **106**, 251901 (2015).
- ³⁹S. Xiao, G. Ma, Y. Li, Z. Yang, and P. Sheng, *Appl. Phys. Lett.* **106**, 091904 (2015).
- ⁴⁰Z. Chen, C. Xue, L. Fan, S.-y. Zhang, X.-j. Li, H. Zhang, and J. Ding, *Sci. Rep.* **6**, 30254 (2016).
- ⁴¹A. Allam, A. Elsabbagh, and W. Akl, *J. Acoust. Soc. Am.* **140**, 3607 (2016).
- ⁴²B.-I. Popa, L. Zigoneanu, and S. Cummer, *Phys. Rev. B* **88**, 024303 (2013).
- ⁴³B.-I. Popa, D. Shinde, A. Konneker, and S. A. Cummer, *Phys. Rev. B* **91**, 220303 (2015).
- ⁴⁴V. Fokin, M. Ambati, C. Sun, and X. Zhang, *Phys. Rev. B* **76**, 144302 (2007).

- ⁴⁵R. Simovski, Opt. Spectrosc. **107**, 726 (2009).
- ⁴⁶A. Alù, Phys. Rev. B **83**, 081102 (2011).
- ⁴⁷A. Srivastava, International Journal of Smart and Nano Materials **6**, 41 (2015).
- ⁴⁸X. Hu, K.-M. Ho, C. T. Chan, and J. Zi, Phys. Rev. B **77**, 172301 (2008).
- ⁴⁹M. Yang, G. Ma, Y. Wu, Z. Yang, and P. Sheng, Phys. Rev. B **89**, 064309 (2014).
- ⁵⁰J. N. Reddy, *Mechanics of Laminated Composite Plates and Shells: Theory and Analysis, Second Edition* (CRC Press, Boca Raton, 2004) pp. 269, 356-357.
- ⁵¹C. K. Lee, J. Acoust. Soc. Am. **87**, 1144 (1990).
- ⁵²ASTM E2611 - 09, "Standard Test Method for Measurement of Normal Incidence Sound Transmission o Rep. (ASTM International, 2009).
- ⁵³P. Li, S. Yao, X. Zhou, G. Huang, and G. Hu, J. Acoust. Soc. Am. **135**, 1844 (2014).
- ⁵⁴Z.-m. Gu, B. Liang, Y. Li, X.-y. Zou, L.-l. Yin, and J.-c. Cheng, J. Appl. Phys. **117**, 074502 (2015).
- ⁵⁵M. Abom, Mech. Syst. Signal Pr. **5**, 89 (1991).

ACCEPTED MANUSCRIPT

